Closed-loop impedance modeling and analysis of three-phase active rectifier below 150 kHz frequency range

Zhongting Tang*, Flemming Johansen**, and Pooya Davari*
*AAU Energy, Aalborg University, Aalborg 9220, Denmark
** Schneider Electric IT Denmark, DK-6000 Kolding
E-mails: zta@energy.aau.dk, flemming.johansen@se.com, pda@energy.aau.dk
URL: www.se.com

ACKNOWLEDGMENT

This work was supported by the CLEAN-Power (Compatibility and Low electromagnetic Emission Advancements for Next generation Power electronic systems) project at the Department of Energy, Aalborg University, Aalborg, Denmark, funded by Independent Research Fund Denmark (DFF).

***Index Terms*—closed-loop impedance modeling, three-phase rectifier, EMI, stability, impedance measurement.**

***Abstract*—This paper derives the closed-loop impedance model for the typical three-phase active rectifier and investigates the dominant factors influencing the converter impedance below 150 kHz frequency range from the basic performance (e.g., steady-state and dynamic performance) and EMI perspectives. Therefore, the complete modeling process of the closed-loop impedance is described, including the control analysis and impedance modeling. The discussion of improving basic performances and EMI performance for the power converter is proposed. Moreover, an advanced impedance measurement technique is introduced. Finally, the validation of the derived closed loop impedance model and the dominant influence analysis for the three-phase rectifier are carried out in MATLAB and PLECS.**

I. INTRODUCTION

Impedance modeling of power electronics converters has been studied for many years since it can characterize many converter properties [1], [2]. The two main aspects are the low-frequency related performance (e.g., harmonic distortions below 2 kHz) [3] and high-frequency related performance (i.e., above 150 kHz frequency range) [4]. The low-frequency related performance contains steady-state errors, dynamic performance, power quality, stability, and so on. While the high-frequency related performance is the Electromagnetic Interference (EMI) characteristic, which critically determines the power density of the power converter. That is, the EMI filter are required in the commercial converters, to comply with emission standards. The prior-art research mainly focuses on frequency ranges above 150 kHz as required in many standards (IEC standards) [5]. However, the disturbances caused by the range below 150 kHz increase a lot, especially along with the application of wide bandgap devices in power electronics converters, and the extensive penetration of power electronic converters [6] and Mains Communication Systems (MCS) [7], [8]. Therefore, the EMI performance for the power converter below the 150 kHz frequency range is essential to be characterized, where the Working Group (WG) 8 and joint working group (JWG) 6 of the IEC Technical Committee 77A (TC77A) are standardizing consensus compatibility and emission levels [9].

The nonlinear behavior of semiconductor devices in power electronics converters is the culprit of noise emissions, which always cover broad ranges of frequencies (i.e., both the low-frequency harmonic and high-frequency EMI) [10]. The research gap between 2-150 kHz creates a need to be investigated due to the large-scale grid integration of renewable power generation systems and advanced communication technology (e.g., Mains Communication Systems (MCS)). On one hand, the renewable integration threatens the harmonic stability and power quality of the power grid, especially connected to a weak grid (i.e., high grid impedance) [11]. Thus, many impedance modeling techniques and control methods have been proposed to characterize the performance above 2 kHz considering the grid-connected condition [10], [12], [13]. On the other hand, the EMI emissions below 150 kHz draw more and more attention, such as the investigation of conducted disturbance [8], analytical modeling of 9-150 kHz EMI [14], and high-

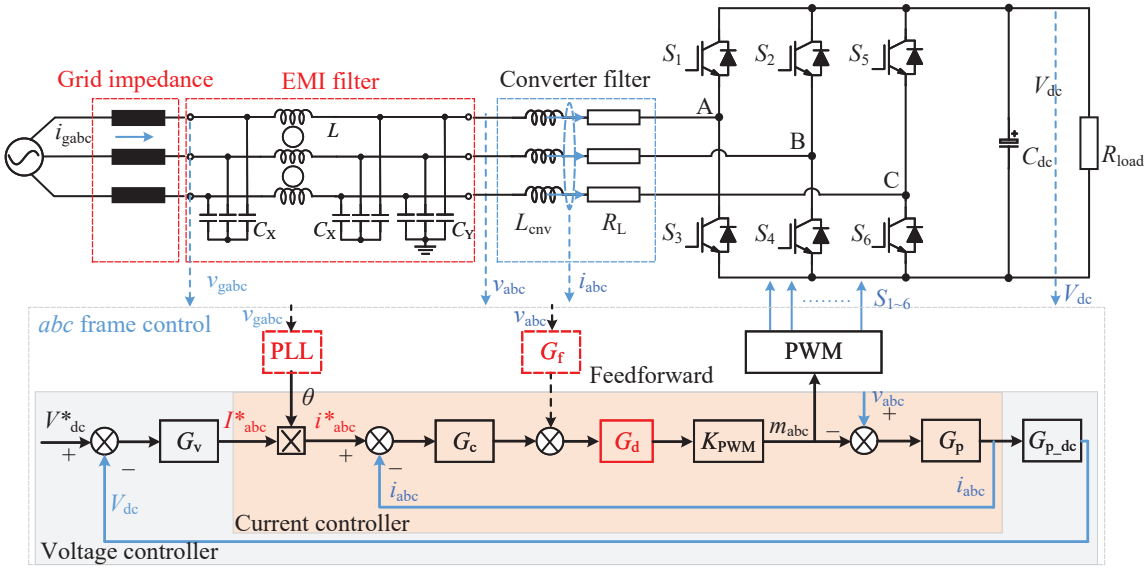

Fig. 1. Block diagram of the three-phase active rectifier with abc frame controller, where v_{gabc} and i_{gabc} are the grid phase voltage and current, v_{abc} and i_{abc} are the phase voltage and current after the EMI filter, L_{cnv} and R_L are the input filter and its equivalent series resistance (ESR), $S_{1\text{-}6}$ are the semiconductor devices of the rectifier, V_{dc} is the DC-link voltage, C_{dc} is the DC-link capacitor, and R_{load} is the output load.

frequency (2–150 kHz) distortion measurement in low-voltage networks [15].

The impedance behavior of the power converter is determined by the passive components (e.g., the input EMI filter, and the grid impedance) and parasitic components as well as the closed-loop control. That is the controller design is a solution to adjust the impedance behavior of the power converter, ensuring good steady-state and dynamic performance [16]. Thus, it is vital to characterize the converter impedance performance within the frequency range below 150 kHz to have a trade-off between control and EMI filter designs. For instance, literature [17] discusses the impedance analysis of the single-phase PFC converter in the frequency range of 0-150 kHz from the power quality and EMI performance perspective [18]. Thus, this paper will further highlight the importance of the closed-loop impedance modeling, and analyze the dominant factors relating to the converter impedance below 150 kHz frequency range from control performance and EMI perspectives. Moreover, the research objective is the three-phase active rectifier, which is typical and widely used in many fields (i.e., such as EV chargers, motor drives, UPS systems, etc.) [16].

The control analysis and closed-loop impedance modeling in the stationary frame linear current regulator have been presented in Section II. The impact factors for the converter impedance have been discussed in Section III, such as controller parameters, delay time, PLL, and passive components. In addition, Section IV proposed an advanced impedance measurement technique and its implementation process. Validation of the analytical model and measurements is carried out in Section V. Finally, Section VI gives the conclusion.

II. Closed-Loop Impedance Modeling

Fig. 1 shows the schematic of the three-phase active rectifier as well as the closed-loop control block in the stationary frame, i.e., abc linear control. The schematic presents the grid source, the grid impedance, the EMI filter, the converter input filter, the six-switch boost three-phase active rectifier, and the output capacitor and load. Moreover, the abc frame control adopts the typical double closed-loop controller, i.e., the voltage control outer loop and the current control inner loop. The voltage error from the comparison of the DC-link voltage reference and feedback (V^*_{dc} and V_{dc}) goes through a voltage controller G_v, and then generates the amplitude of the reference current I^*_{abc}. Combined with the phase angle θ, the reference current i^*_{abc} is achieved and goes through a current controller G_c and the converter gain K_{PWM} to obtain the duty cycle of abc phases, outputting control signals for switches by the pulse width modulation (PWM). The phase-locked loop (PLL) and the feedforward part are optional parts

discussed in the following, when the active rectifier operates under different conditions.

Since the voltage controller G_{v} impacts the impedance in a very low-frequency range, and couples with the PLL in the abc frame, the impact factors of G_{v} and PLL will be discussed separately. Thus, the basic current closed-loop transfer functions are derived firstly as below:

$$G_{\mathrm{op\_c}} = G_{\mathrm{c}} G_{\mathrm{d}} K_{\mathrm{PWM}} G_{\mathrm{P}} \tag{1}$$

$$G_{\mathrm{cl\_c}} = \frac{G_{\mathrm{op\_c}}}{G_{\mathrm{op\_c}} + 1} = \frac{G_{\mathrm{c}} G_{\mathrm{d}} K_{\mathrm{PWM}} G_{\mathrm{P}}}{G_{\mathrm{c}} G_{\mathrm{d}} K_{\mathrm{PWM}} G_{\mathrm{P}} + 1} \tag{2}$$

where $G_{\mathrm{op\_c}}$, $G_{\mathrm{cl\_c}}$ are the open loop and closed loop transfer functions of the current controller, respectively, G_{d} is the delay part caused by the sampling and modulation, and G_{P} is the transfer function of the converter plant. The current loop controller G_{c} adopts an advanced proportional-integral (PI) controller with the low-frequency suppression, avoiding the impact of the DC bias generated by the current sensor (i.e., the zero drift). It can be expressed as

$$G_{\mathrm{c}} = k_{\mathrm{pi}} + \frac{k_{\mathrm{ii}}}{s + \omega_{\mathrm{s}}} \tag{3}$$

where k_{pi} and k_{ii} are the proportional and integral parameters, respectively, and ω_{s} is the parameter determining the frequency range of the low-frequency suppression. It should be noted that ω_{s} is less than the grid angle frequency, i.e., $\omega_{\mathrm{g}} = 2\pi f_{\mathrm{g}}$, and $f_{\mathrm{g}} = 50Hz$. Thus, the current controller can work well in the sinusoidal system of 50 Hz in practice. Compared to the proportional resonant (PR) controller, the advanced PI controller is less sensitive to the grid frequency, which means less affected by frequency accuracy.

Moreover, the converter gain K_{PWM} and G_{P} are decided by system parameters. K_{PWM} is $V_{\mathrm{dc}}/2$ in the three-phase active rectifier, and the system plant is

$$G_{\mathrm{P}} = \frac{1}{L_{\mathrm{cnv}} s + R_{\mathrm{L}}} \tag{4}$$

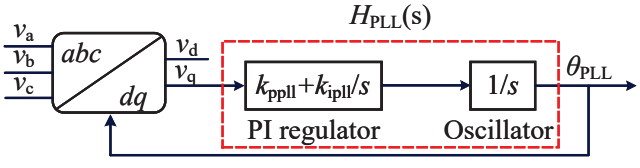

Fig. 2. Block diagram of SRF-PLL.

Thus, the closed-loop transfer function is

$$G_{\mathrm{cl\_c}} = \frac{\frac{V_{\mathrm{dc}}(k_{\mathrm{pi}} s + k_{\mathrm{pi}}\omega_{\mathrm{s}} + k_{\mathrm{ii}}) G_{\mathrm{d}}}{2(s+\omega_{\mathrm{s}})(L_{\mathrm{cnv}} s + R_{\mathrm{L}})}}{\frac{V_{\mathrm{dc}}(k_{\mathrm{pi}} s + k_{\mathrm{pi}}\omega_{\mathrm{s}} + k_{\mathrm{ii}}) G_{\mathrm{d}}}{2(s+\omega_{\mathrm{s}})(L_{\mathrm{cnv}} s + R_{\mathrm{L}})} + 1} \tag{5}$$

which can be used to analyze the bandwidth and stability of the three-phase active rectifier.

A. Basic closed-loop impedance

According to the current controller (the red part) in Fig. 1, the transfer function equation can be derived as

$$\boldsymbol{V}_{\mathrm{abc}} - (i^{*}_{\mathrm{abc}} + \boldsymbol{I}_{\mathrm{abc}}) G_{\mathrm{c}} G_{\mathrm{d}} K_{\mathrm{PWM}} = \frac{\boldsymbol{I}_{\mathrm{abc}}}{G_{\mathrm{P}}} \tag{6}$$

where $V_{\mathrm{abc}}(s)$ and $I_{\mathrm{abc}}(s)$ only represent the voltage and current of one phase in the abc frame (e.g., $V_{\mathrm{abc}}(s)/I_{\mathrm{abc}}(s) = V_{\mathrm{a}}(s)/I_{\mathrm{a}}(s)$). Thus, the closed-loop impedance can be achieved as

$$Z_{\mathrm{in}} = \frac{\boldsymbol{V}_{\mathrm{abc}}}{\boldsymbol{I}_{\mathrm{abc}}} = \frac{1}{G_{\mathrm{P}}} + G_{\mathrm{c}} G_{\mathrm{d}} K_{\mathrm{PWM}} \tag{7}$$

Among Eq. 7, the transfer function of the delay is

$$G_{\mathrm{d}} = e^{-sT_{\mathrm{d}}} \tag{8}$$

where T_{d} is the delay time.

B. Closed-loop impedance with PLL

When considering the PLL part, the closed-loop impedance can be built as

$$Z_{\mathrm{in}}|_{\mathrm{PLL}} = \frac{\boldsymbol{V}_{\mathrm{abc}}}{\boldsymbol{I}_{\mathrm{abc}}} = \frac{\frac{1}{G_{\mathrm{P}}} + G_{\mathrm{c}} G_{\mathrm{d}} K_{\mathrm{PWM}}}{1 + I^{*}_{\mathrm{abc}} G_{\mathrm{PLL}} G_{\mathrm{c}} G_{\mathrm{d}} K_{\mathrm{PWM}}} \tag{9}$$

In the three-phase active rectifier, the synchronous reference frame phase locked loop (SRF-PLL) is adopted, as shown in Fig. 2. The SRF-PLL regulator composes of a PI controller and an oscillator, and the input grid voltages are measured and transformed by $T_{\mathrm{abc/dq}}$. The transfer function of $H_{\mathrm{PLL}}(s)$ is expressed as

$$H_{\mathrm{PLL}}(s) = (k_{\mathrm{ppll}} + \frac{k_{\mathrm{ipll}}}{s}) \frac{1}{s} \tag{10}$$

where k_{ppll} and k_{ipll} are the control parameters of the PI controller in Fig. 2. Since the impact factors are discussed one by one, the transfer function of the PLL (i.e., G_{PLL}) is defined as an uniform expression without considering the coupling of the grid voltage when the grid impedance is zero [19].

$$G_{\mathrm{PLL}}(s) = \frac{1}{2} \frac{H_{\mathrm{PLL}}(s)}{1 + V_{\mathrm{m}} H_{\mathrm{PLL}}(s)} \tag{11}$$

where V_{m} is the amplitude of the grid voltage.

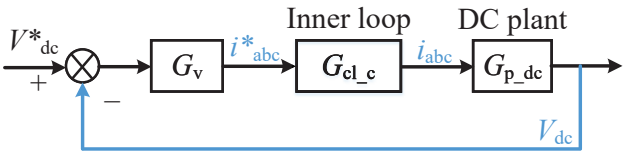

Fig. 3. Double loop block considering the outer loop DC plant, where $G_{\text{p\_dc}}$ is the transfer function of the DC plant.

C. Closed-loop impedance with G_v

Fig. 3 simplifies the control block diagram when considering the outer voltage controller. The open loop transfer function can be expressed as

$$G_{\text{op\_v}} = G_{\text{v}} G_{\text{cl\_c}} G_{\text{P\_dc}} \tag{12}$$

According to Figs. 1 and 3, the transfer function equation of the closed-loop voltage controller can be depicted as

$$\boldsymbol{V}_{\text{abc}} G_{\text{P}} - ((V^*_{\text{dc}} + \boldsymbol{I}_{\text{abc}} G_{\text{P\_dc}}) G_{\text{v}} + \boldsymbol{I}_{\text{abc}}) G_{\text{op\_c}} = I_{\text{abc}} \tag{13}$$

And the closed-loop impedance can be derived as

$$Z_{\text{in}}|_{\text{Gv}} = \frac{\boldsymbol{V}_{\text{abc}}}{\boldsymbol{I}_{\text{abc}}} = \frac{1 + G_{\text{op\_c}} + G_{\text{op\_c}} G_{\text{v}} G_{\text{P\_dc}}}{G_{\text{P}}} \tag{14}$$

in which the voltage controller is the typical PI controller

$$G_{\text{v}} = k_{\text{pv}} + \frac{k_{\text{iv}}}{s} \tag{15}$$

And the transfer function of the DC plant is

$$G_{\text{P\_dc}} = \frac{3V_{\text{m}}}{4V_{\text{dc}} C_{\text{dc}} s} \tag{16}$$

where V_{dc} here is considered as a constant value, being equal to the reference DC link voltage. It should be noted that the coupling of the DC link voltage outer loop and the current inner loop is neglected since only one factor (i.e., the outer loop voltage controller) has been considered in the closed-loop impedance.

D. Closed-loop impedance with passive components

Referring to the effect of the passive component (e.g., the grid impedance or EMI filter), the closed-loop impedance should integrate the input impedance of the passive component into the developed Z_{cnv} models following Middlebrook extra element theorem [20]. As shown in Fig. 4(a), the closed-loop impedance considering the passive component can be derived as:

$$Z_{\text{in}}|_{\text{filter}} = Z_{\text{iP}\infty} \frac{1 + \frac{Z_{\text{oP0}}}{Z_{\text{cnv}}}}{1 + \frac{Z_{\text{oP}\infty}}{Z_{\text{cnv}}}} \tag{17}$$

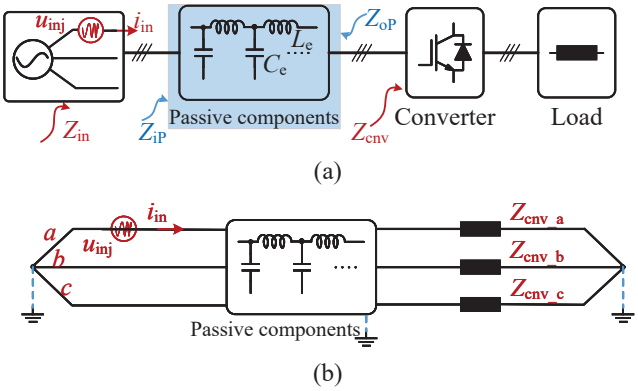

Fig. 4. Circuit Schematic of the impedance measurement in the three-phase active rectifier, (a) impedance measurement considering passive components, and (b) impedance calculation with different connections.

where Z_{cnv} is the closed-loop impedance of the power converter, $Z_{\text{iP}\infty}$ is the input impedance of the passive component with the output port open, $Z_{\text{oP}\infty}$ the output impedance of the passive component with the input port open, and Z_{oP0} the output impedance of the passive component with the input port shorted.

It should be noted that the result of the impedance measurement are different when the neutral point has different linking ways. As shown in Fig. 4(b), when the neutral points of the grid, the passive component and the converter are connected, the measurement impedance Z_{inm} is equal to $V_{\text{abc}}(s)/I_{\text{abc}}(s) = V_{\text{a}}(s)/I_{\text{a}}(s)$. While Z_{inm} is equal to $1.5V_{\text{abc}}(s)/I_{\text{abc}}(s) = 1.5V_{\text{a}}(s)/I_{\text{a}}(s)$ if all the neutral points are floating.

III. Performance Analysis

To investigate the dominant factors influencing the converter impedance below 150 kHz frequency range, the system parameters of the three-phase active rectifier are shown in Table I. It should be noted that only one factor will be changed at once when analyzing the impedance and basic performance.

A. Control performance

As to control parameters, the bode diagrams of the open loop transfer function of the current and voltage controller are shown in Fig. 5. The control parameters always impact the basic performance in dynamic response, stability, power quality, and control accuracy, which have been described in bandwidth (Bw), phase margin (Pm), total harmonic distortion (THD) and steady-state error (Err). It can be shown in Fig. 5(a) both k_{pi} and k_{ii} affect the bandwidth of the current controller, being positively correlated and k_{pi} acts the dominant

TABLE I
SYSTEM PARAMETERS OF THREE-PHASE ACTIVE RECTIFIER

Symbol	Parameter	Value
V_{abc}, V_a	Grid phase voltage	230 Vrms
V_{dc}	DC link voltage	800 V
f_g	Grid frequency	50 Hz
L_{cnv}	Converter boost filter	2 mH
R_L	ESR of L_{cnv}	0.2 Ω
C_{dc}	DC link capacitor	1000 uF
f_s	switching frequency	20 kHz
T_s	Sampling time	1/40000 s
R_{load}	Load resistor	80 Ω

role. Moreover, large k_{pi} and k_{ii} will generate current oscillations on the converter filter, decreasing the THD of i_{abc}. k_{ii} determines the steady-state error since the error of 11% can be achieved in Fig. 5(a). Fig. 5(b) shows the bode diagram of the voltage controller. It illustrates that the outer voltage controller can almost remove the steady-state error, and the control parameters only impact the dynamic performance of the rectifier. Actually, the control parameters of the double-loop controller should be regulated together to achieve an optimal dynamic and steady-state performance [16].

B. Impedance performance

Figs. 6-8 illustrate the closed-loop impedance of the rectifier based on Eqs. 7, 9, and 14 analytical models. The main factors discussed for the impedance performance in this paper include control parameters, the PLL, the delay, and passive components as follows.

(1) **Control parameters:** Fig. 6 shows the analytical closed-loop impedance model with different control parameters. The basic impedance model (only considering the current control loop) as Eq. 7 is presented in Fig. 6a, which shows that the control parameters of G_c impact the impedance performance in the frequency range of 0-20 kHz (below the switching frequency). While Fig. 6(b) draws the impedance with the DC-link voltage controller. It can be seen the parameters in G_v can change the impedance in the frequency below 1 kHz.

(2) **PLL:** According to Eq. 9, the closed-loop impedance with the PLL has been shown in Fig. 7(a). It can be illustrated that the impedance performance in the frequency range of 0-4 kHz is related to the parameters in the PLL. Inevitably, the PLL will impact the low-frequency stability of grid-connected systems [19].

(3) **Delay:** The delay part exists in the practice in the control period, e.g., controller computation, sampling and modulation. It should be considered when designing

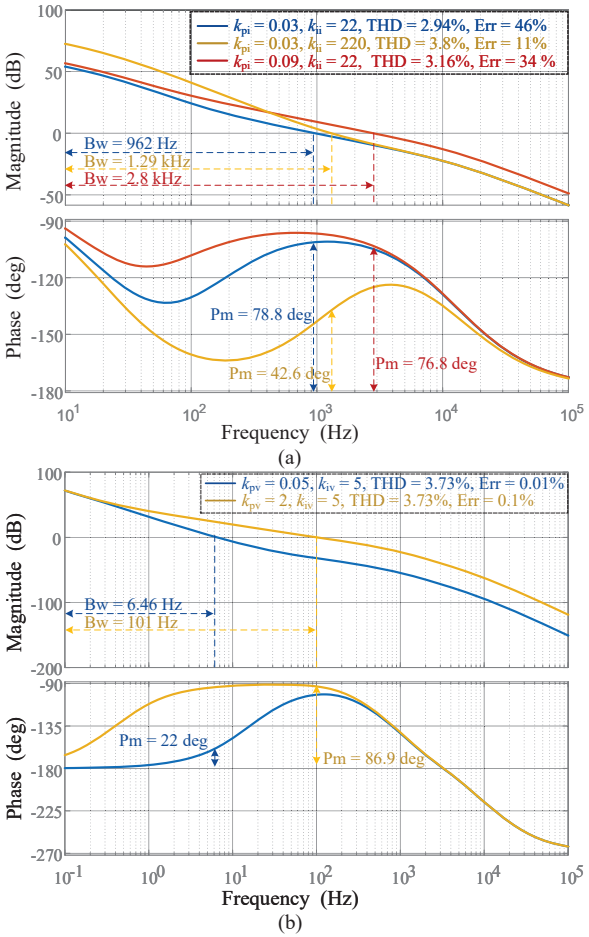

Fig. 5. Bode diagram of the open loop transfer function with different control parameters, (a) G_{op_c} with different k_{pi} and k_{ii}, and (b) G_{op_v} with different k_{pv} and k_{iv}.

the controller to avoid the stability issue. Fig. 7(b) depicts that the delay impacts the impedance in the frequency range of 200 Hz-20 kHz, in which the delay time T_d is several times the sampling period T_s.

(4) **Passive components:** The input passive component of the three-phase active rectifier considers the grid impedance and the EMI filter. From the perspective of CM noise suppression and rectifier stability, the control and EMI filters should be designed together according to specific system technical requirements. Besides, the controller design will leave a certain margin for the grid impedance, which means the rectifier can operate under certain conditions of weak grid. It can be seen in Fig. 8 that the passive components (both the grid impedance and EMI filters) dominates the impedance behavior in the frequency range of 2-150 kHz. Moreover, Fig. 8(b) illustrates the EMI filter impacts the stability since the resonance point and its damping change along

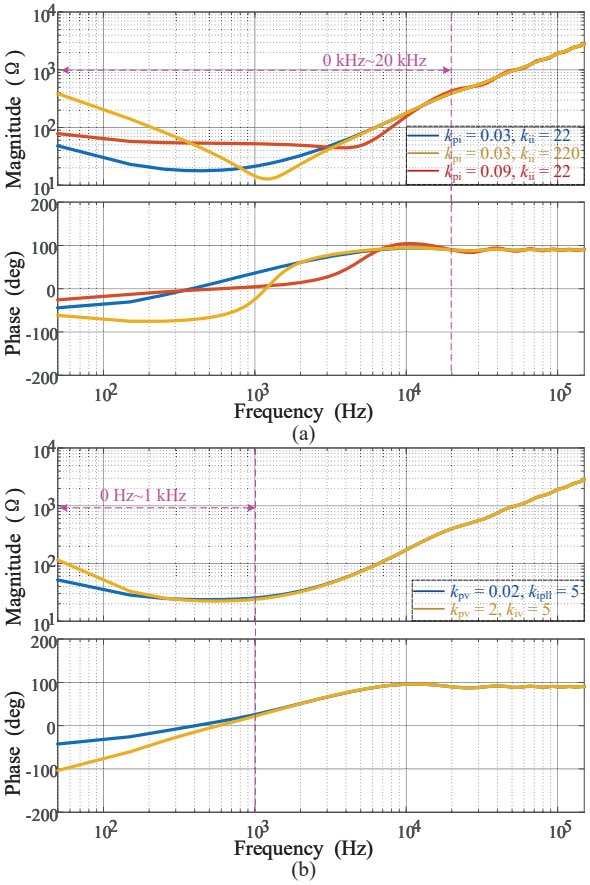

Fig. 6. Effect of control parameters on the closed-loop impedance of the three-phase rectifier, (a) different current control parameters (k_{pi}, k_{ii}), and (b) different voltage control parameters (k_{pv}, k_{iv}).

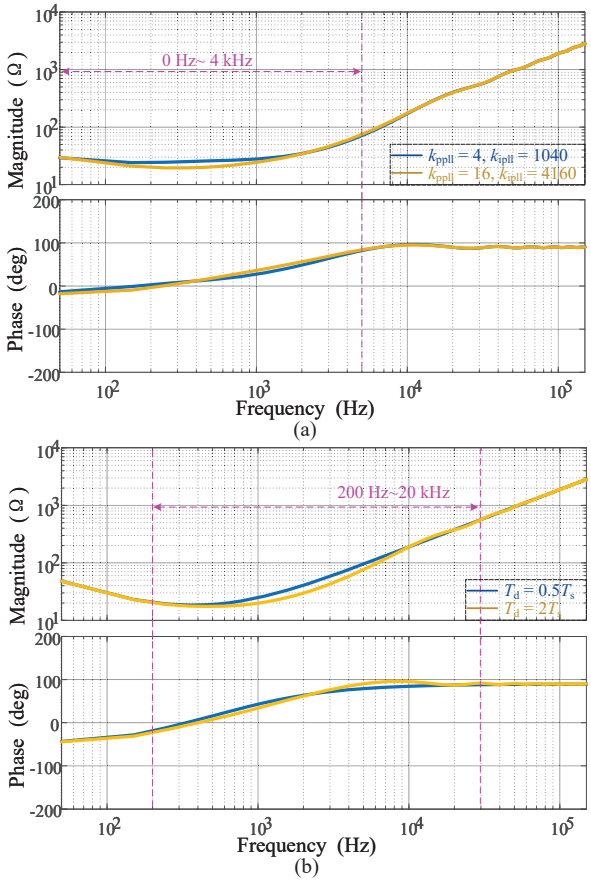

Fig. 7. Impact of the PLL and the delay on closed-loop impedance of the three-phase active rectifier, (a) different control parameters in the PLL (k_{ppll} and k_{ipll}), and (b) different delay times (T_{d}).

with different EMI filters.

IV. Impedance Measurement

Before validating the analytical models of the closed-loop impedance for power converters, an improved fast impedance measurement method is presented. Fig. 9 (a) shows the flowchart of the impedance calculation. The first step is setting the multitone signal at the input of the three-phase active rectifier as depicted as Fig. 4. Then, the data of the input voltage and current (both in simulation and experiment) are captured to calculate the input impedance in the frequency domain by MATLAB FFT function.

As to the injected signal, a multi-tone signal is selected with multiple frequency points to achieve fast frequency sweeping in a large frequency range. Fig. 9 (b) presents the time and frequency domain waveforms of the multi-tone signal, which contains 46 frequency points covering up to 150 kHz frequency range. The multi-tone signal can be expressed as:

$$u_{\mathrm{inj}}(t) = \sqrt{\frac{2}{N_{\mathrm{tones}}}} \sum_{k=1}^{N_{\mathrm{tones}}} sin(\omega_{\mathrm{k}} t + \theta_{\mathrm{k}}) \tag{18}$$

$$\omega_{\mathrm{k}} = 2\pi k f_{\mathrm{b}}, \theta_{\mathrm{k}} = \frac{\pi(k-1)^2}{N_{\mathrm{tones}}} \tag{19}$$

where N_{tones} is the frequency points, f_{b} is the base frequency. In fig. 9(b), N_{tones} is equal to 46, and f_{b} is chosen as 53 Hz to avoid interference with the three-phase active rectifier (the grid frequency f_{g} is 50 Hz).

V. Validation

Validation of the analytical closed-loop impedance models has been carried out alined with the dominant factors in Section III.B. The three-phase active rectifier system (with the parameters in Table I) is simulated in PLECS as well as the advanced impedance measurement.

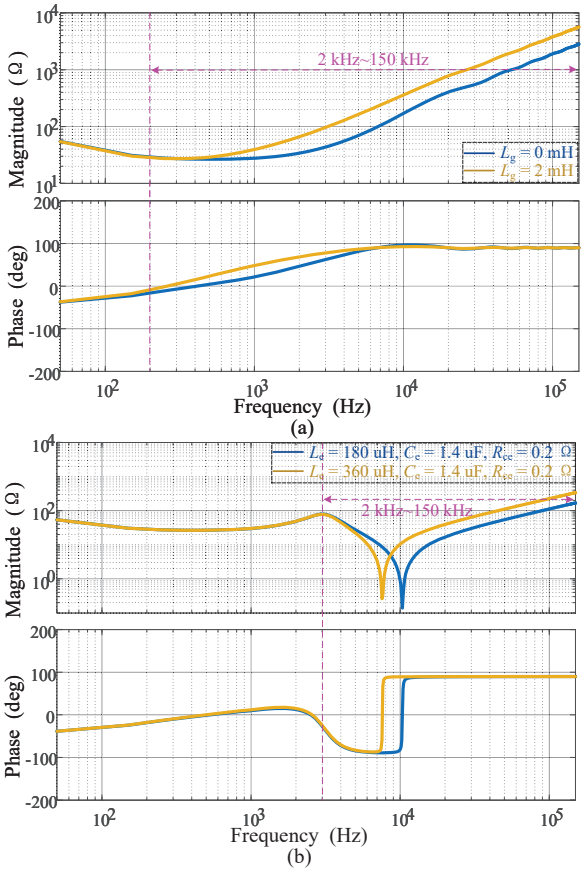

Fig. 8. Effect of passive components on closed-loop impedance of the three-phase active rectifier, (a) different grid impedances, and (b) different EMI filters, where L_e and C_e are the inductor and capacitor of one stage EMI filter.

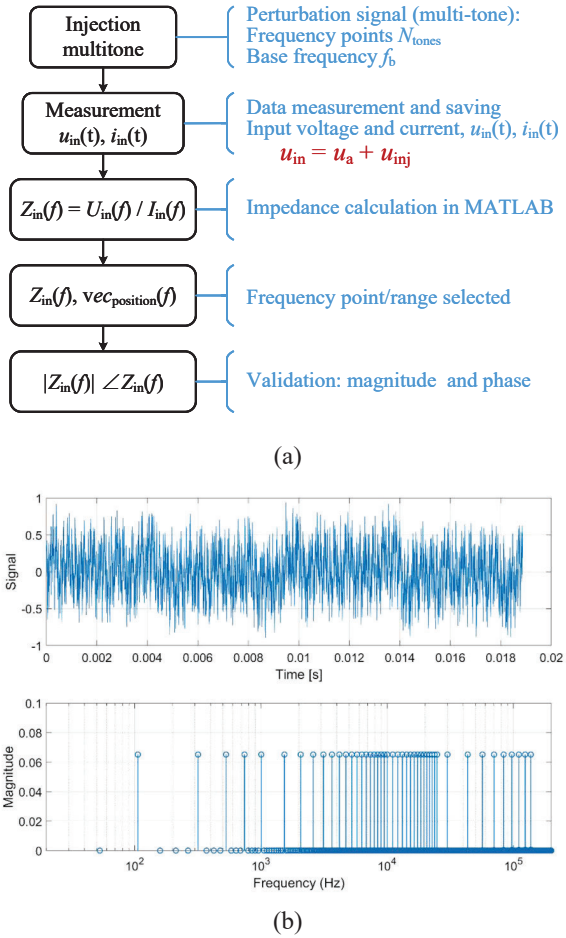

Fig. 9. Advanced impedance measurement technique, (a) flowchart of impedance calculation in MATLAB, and (b) injected signals.

The validation results are shown in Figs. 10-12, in which the measurements agrees well with the analytical models in Figs. 6-8. Fig. 10 shows the validation performance under different control parameters, in which there is a slight mismatch in very low frequency when k_{pv} and k_{iv} are high. It reveals that the coupling between the outer voltage control and the inner sinusoidal current control cannot be neglected with some control parameters ranges. Since the three-phase active rectifier is widely used in grid-connected systems, the PLL must be considered. Fig. 11 shows the comparison of the measurement and the models with different parameters (k_{ppll} and k_{ipll}) in the PLL and different delay time (T_d). The frequency range of the impedance impacted by those two factors is below the control frequency range, which means the controller can intervene the impactness.

To further validate the accuracy of the closed-loop impedance model with passive components, two more measurements including the grid impedance and the EMI filter are conducted. Fig. 12 (a) shows comparative results when the grid impedance is involved, which reveals that the input passive inductor $L = L_g + L_{cnv}$ dominates the impedance behavior beyond the bandwidth of the controller, and and the boost inductor dominates behavior untill its phase reaches $+90$ degrees. Fig. 12 (b) is the result that a one stage EMI filter as shown in Fig. 4 is placed in front of the three-phase rectifier. As explained in Eq. 17, applying Middlebrook theorem the effect of the EMI filter is included in the impedance model. It can be seen the EMI filter inductance dominates the impedance behavior at higher frequencies (i.e., 2-150 kHz).

VI. Conclusion

In this paper, the closed-loop impedance modeling process for the three-phase active rectifier is developed considering the control calculation delay, the PLL, the inner current control loop, the outer voltage controller,

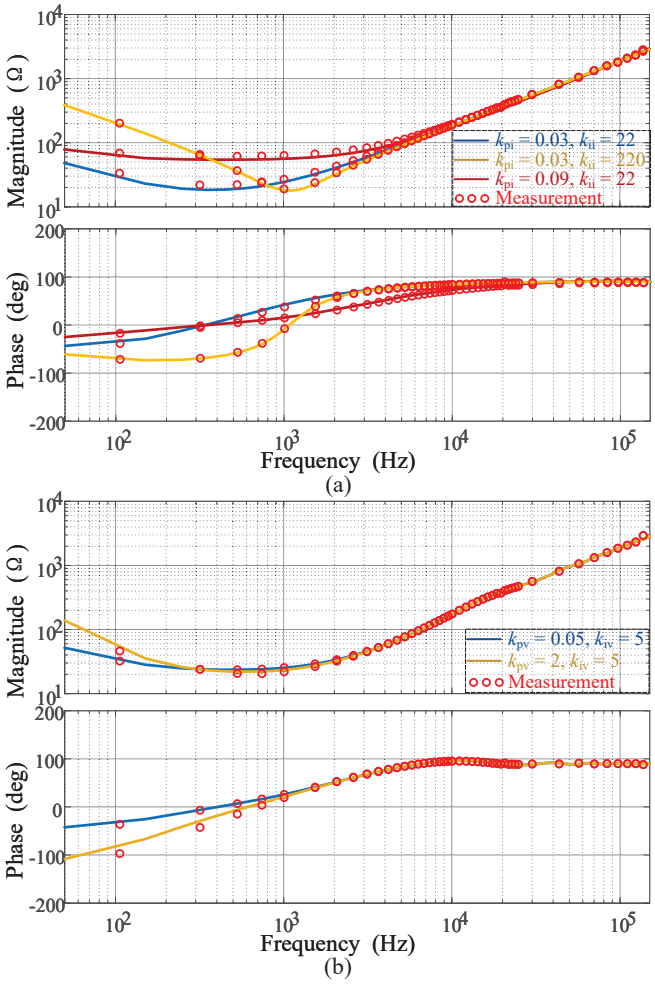

Fig. 10. Measurement results versus closed-loop impedance models of the rectifier under different control parameters, different current control parameters, and (b) different voltage control parameters.

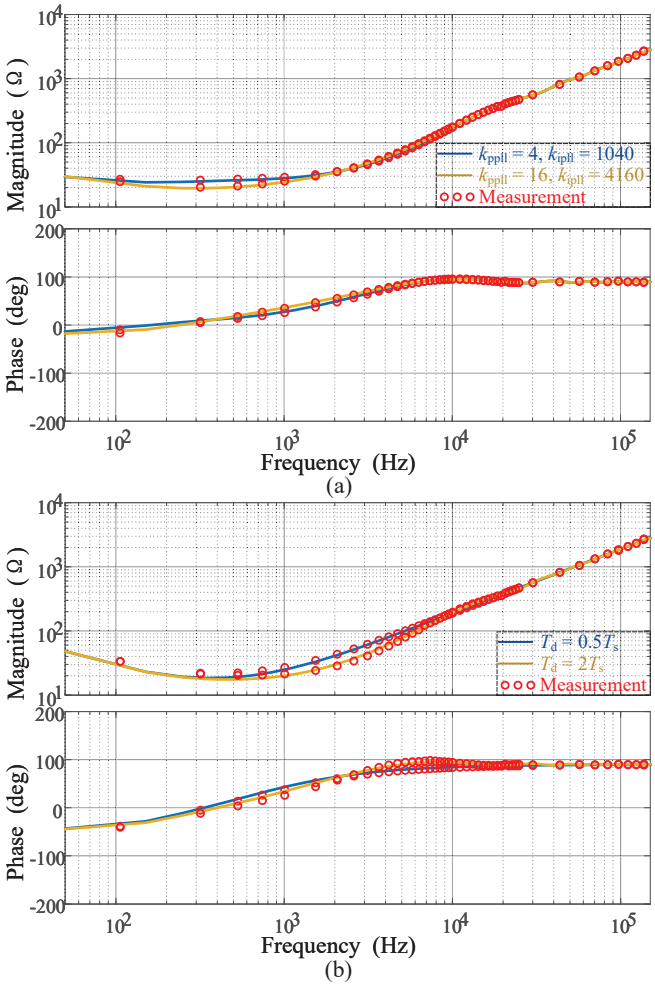

Fig. 11. Validation of measurements and analytical impedance model of the rectifier considering the PLL and the delay, (a) different control parameters in the PLL, and (b) different delay times.

and the passive components. Considering the upcoming emission standard, the investigations of the dominant impact factors for the impedance behavior are focused on frequency range below 150kHz. That can guide how to adjust the impedance to avoid its adverse effect on the emission/signals within different frequency ranges. Moreover, an improved impedance measurement is proposed to fast capture the impedance information in a wide frequency range. The investigation of impedance of the three-phase rectifier, is done on a control system implemented in the abc frame, and future investigations could be extended to dq and $\alpha\beta$ frames.

REFERENCES

[1] H. Zhang, L. Yang, S. Wang and J. Puukko, "Common-mode EMI noise modeling and reduction with balance technique for three-level neutral point clamped topology," IEEE Trans. Ind. Electron., vol. 64, no. 9, pp. 7563-7573, Sep. 2017.

[2] S. Shah and L. Parsa, "Impedance modeling of three-phase voltage source converters in DQ, sequence, and phasor domains," IEEE Trans. Energy Convers., vol. 32, no. 3, pp. 1139-1150, Sep. 2017.

[3] Y. Liao, Z. Liu, H. Zhang and B. Wen, "Low-frequency stability analysis of single-phase system with dq-frame impedance approach—part I: impedance modeling and verification," IEEE Trans. Ind. Appl., vol. 54, no. 5, pp. 4999-5011, Sep.-Oct. 2018.

[4] M. Moreau, N. Idir and P. Le Moigne, "Modeling of conducted EMI in adjustable speed drives," IEEE Electromagn. Compat., vol. 51, no. 3, pp. 665-672, Aug. 2009.

[5] Electromagnetic Compatibility (EMC) Part 3-2: Limits-Limits for Harmonic Current Emissions (Equipment Input Current $\leq$ 16 A per Phase), I. I. E. Commission, Geneva, Switzerland, 2001. Consol. Ed. 2.1.

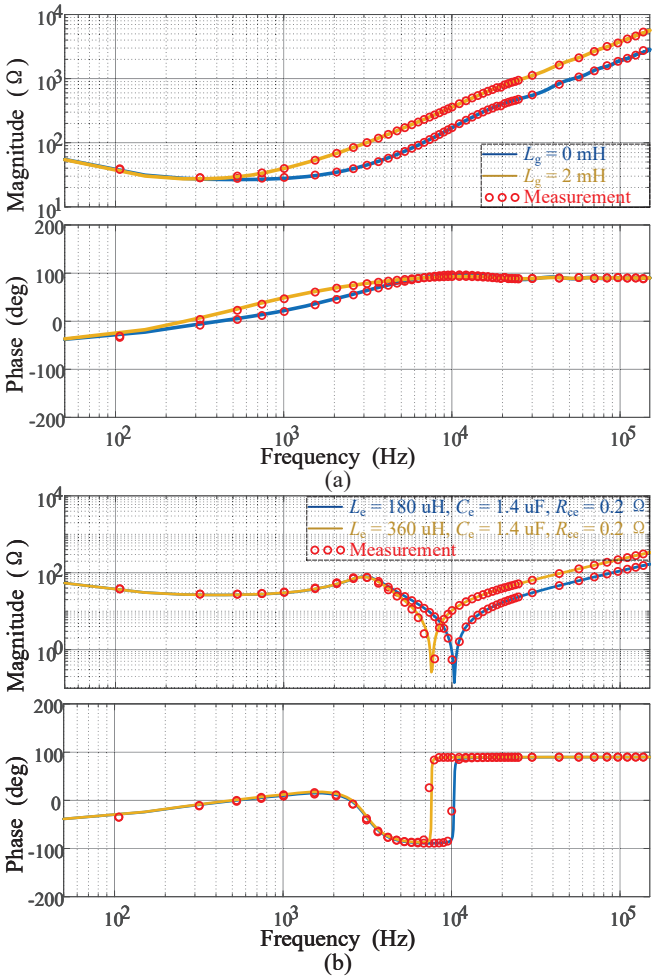

Fig. 12. Validation of the measurements and analytical model of the rectifier under different passive components paramters, (a) different grid impedances, and (b) different EMI filters.

[6] Y. Zhang, H. Wang, Z. Wang, F. Blaabjerg and M. Saeedifard, "Mission Profile-based System-Level Reliability Prediction Method for Modular Multilevel Converters," IEEE Trans. Power Electron., vol. 35, no. 7, pp. 6916 - 6930, Jul. 2020.

[7] P. Kotsampopoulos et al., "EMC issues in the interaction between smart meters and power-electronic interfaces," IEEE Trans. Power Deliv., vol. 32, no. 2, pp. 822-831, Apr. 2017.

[8] "Assessment of conducted disturbances above 2 kHz in MV and LV power systems," Cigre, reference 799, Apr. 2020.

[9] IEC 61000-2-2:2002+AMD1:2017+AMD2:2018 CSV Electromagnetic compatibility (EMC) - Environment - Compatibility levels for low-frequency conducted disturbances and signalling in public low-voltage power supply systems (standard compatibility levels for public LV network).

[10] K. G. Khajeh, D. Solatialkaran, F. Zare and N. Mithulananthan, "Harmonic analysis of multi-parallel grid-connected inverters in distribution networks: emission and immunity issues in the frequency range of 0-150 kHz," IEEE Access, vol. 8, pp. 56379-56402, 2020.

[11] X. Wang and F. Blaabjerg, "Harmonic stability in power electronic-based power systems: concept, modeling, and analysis," IEEE Trans. Smart Grid, vol. 10, no. 3, pp. 2858-2870, May 2019.

[12] M. Cespedes and J. Sun, "Impedance modeling and analysis of grid-connected voltage-source converters," IEEE Trans. Power Electron., vol. 29, no. 3, pp. 1254-1261, Mar. 2014.

[13] J. Yaghoobi, F. Zare, T. Rehman, and H. Rathnayake, "Analysis of high frequency harmonics in distribution networks: 9-150 kHz," in Proc. IEEE ICIT, 2019, pp. 1-6.

[14] N. N. Esfetanaj, Y. Peng, H. Wang, F. Blaabjerg and P. Davari, "Analytical modeling of 9-150 kHz EMI in three-phase active rectifiers," in Proc. IEEE COMPEL, Aalborg, 2020, pp. 1-6.

[15] E. O. A. Larsson, M. H. J. Bollen, M. G. Wahlberg, C. M. Lundmark and S. K. Rönnberg, "Measurements of high-frequency (2–150 kHz) distortion in low-voltage networks," IEEE Trans. Power Deliv., vol. 25, no. 3, pp. 1749-1757, Jul. 2010.

[16] M. Liserre, F. Blaabjerg and S. Hansen, "Design and control of an LCL-filter-based three-phase active rectifier," IEEE Trans. Ind. Appl., vol. 41, no. 5, pp. 1281-1291, Sep.-Oct. 2005.

[17] P. Davari and F. Blaabjerg, "Impedance analysis of single-phase PFC converter in the frequency range of 0–150 kHz," in Proc. IEEE-ECCE Asia, 2022, pp. 2522-2528.

[18] P. T. Jensen and P. Davari, "Power Converter Impedance and Emission Characterization Below 150 kHz," 2021 IEEE International Joint EMC/SI/PI and EMC Europe Symposium, Raleigh, NC, USA, 2021, pp. 255-260.

[19] Y. Wang, X. Chen, Y. Zhang, J. Chen and C. Gong, "Impedance influence analysis of phase-locked loops on three-phase grid-connected inverters," in Proc. IEEE-ECCE Asia, Japan, 2018, pp. 1177-1182.

[20] Middlebrook R. D., " Null double injection and the extra element theorem," IEEE Trans. Educ., vol. 32, no. 3, pp. 167-180, 1989.